

Spin lifetime in InAs epitaxial layers grown on GaAs

K. L. Litvinenko, B. N. Murdin, and J. Allam

Advanced Technology Institute, University of Surrey, Guildford GU2 7XH, England

C. R. Pidgeon

Department of Physics, Heriot-Watt University, Edinburgh EH14 4AS, Scotland

Tong Zhang, J. J. Harris, and L. F. Cohen

Blackett Laboratory, Imperial College London, Prince Consort Road, London SW7 2BZ, England

D. A. Eustace and D. W. McComb

Materials Department, Imperial College London, Prince Consort Road, London SW7 2AZ, England

(Received 4 May 2006; published 29 August 2006)

We report investigation of the spin relaxation in InAs films grown on GaAs at a temperature range from 77 K to 290 K. InAs is known to have a surface accumulation layer and the depth profile of the concentration and mobility is strongly nonuniform. We have correlated the spin relaxation with a multilayer analysis of the transport properties and find that the surface and the interface with the GaAs substrate both have subpicosecond lifetimes (due to the high carrier concentration), whereas the central semiconducting layer has a lifetime of an order of 10 ps. Even for the thickest film studied (1 μm), the semiconducting layer only carried 30% of the total current (with 10% through the interface layer and 60% through the surface accumulation layer). Designs for spintronic devices that utilize InAs, which is attractive due to its narrow gap and strong Rashba effect, will need to include strategies for minimizing the effects of the surface.

DOI: [10.1103/PhysRevB.74.075331](https://doi.org/10.1103/PhysRevB.74.075331)

PACS number(s): 78.47.+p, 72.25.Rb, 72.10.Fk, 72.25.Fe

I. INTRODUCTION

Spin dynamics in semiconductors have been studied extensively, because of their importance for the development of spintronic devices.¹ Due to its very well established growth and the band-gap energy being within the range of widely available ultrafast Ti:sapphire oscillators, most investigations have been focused on bulk or heterostructures of GaAs-based semiconductors.²

Narrow-gap semiconductors (NGS) are of particular interest in terms of potentially important device applications involving infrared detectors and long-wavelength optoelectronic devices. Additionally very high speed electronic transistor devices have been made from NGS due to their high electron mobility.³ NGS materials could be also very beneficial for designing future spintronic devices because of their strong spin-orbit coupling. The presence of space-charge accumulation or inversion layers at the surfaces of $\text{Hg}_{1-x}\text{Cd}_x\text{Te}$ ($x < 0.3$), InAs, InSb, and $\text{InAs}_{1-x}\text{Sb}_x$ could be used to design a contact with metallic materials without a significant resistance mismatch and consequent need for Schottky barrier.⁴ This makes them potential candidates for applications utilizing spin injection from ferromagnetic metals. The effect of surface accumulation due to a native surface defect above the bulk conduction band edge is known to be particularly strong with InAs (Refs. 5–7) and $\text{Hg}_{1-x}\text{Cd}_x\text{Te}$.⁸ Electron spin relaxation strongly depends on the scattering rate and electron kinetic energy. Thus layers with different carrier concentration and mobility have different spin lifetime and different spin relaxation processes could dominate. In this paper we describe an investigation of the effect of inversion layers on the spin-dynamic properties of InAs films grown on semi-insulating GaAs substrates by molecular-beam epitaxy (MBE).

II. SPIN DYNAMICS

There are three main spin relaxation processes: D'yakonov-Perel' (DP),⁹ Elliot-Yafet (EY),¹⁰ and Bir-Aronov-Pikus (BAP).¹¹ The last one is only significant in p -type semiconductors.

The EY spin relaxation rate in bulk material is given by^{10,12}

$$\frac{1}{\tau_s^{(EY)}} \approx A \alpha^2 \left(\frac{E_k}{E_G} \right)^2 \frac{1}{\tau_p}, \quad (1)$$

where the electron kinetic energy E_k , and the momentum relaxation time τ_p are determined by temperature, concentration, and mobility. (For high concentrations, electron-electron scattering may become more important than mobility scattering.) The band structure determines $\alpha = \gamma(1 - \gamma/2)/(1 - \gamma/3)$, where $\gamma = \Delta/(\Delta + E_G)$, Δ is the spin-orbit splitting of the valence band, and E_G is the fundamental energy gap. A is a dimensionless constant, the value of which depends on the orbital scattering interaction and is predicted to be 6 for ionized impurity scattering and 2 for lattice scattering.¹²

The DP spin relaxation rate in bulk material is given by^{9,12}

$$\frac{1}{\tau_s^{(DP)}} = Q \beta^2 \frac{E_k^3}{\hbar^2 E_G} \tau_p, \quad (2)$$

where $\beta = (4\gamma/\sqrt{3-\gamma})(m/m_0)$ where m is the electron effective mass. Q is a dimensionless factor, predicted to be in the ranges of 0.8–3, depending on the dominant momentum relaxation process.¹² For scattering on ionized impurities and

defects $Q \approx 32/21$, whereas for lattice scattering $Q \approx 96/35$.⁹

In the limit of degenerate statistics the typical electron kinetic energy is given by E_F , the Fermi energy, and in the opposite limit of nondegenerate statistics it is $k_B T$. Therefore the DP dominates at high temperature because of the higher power of T in Eq. (2) than in Eq. (1). For semiconductor material with high electron mobility the EY mechanism dominates only at temperatures below 6 K.¹²

As can be seen from Eqs. (1) and (2) the spin lifetime in the case of the DP relaxation mechanism is inversely proportional to the electron mobility, whereas in the case of the EY mechanism it is linearly proportional. This means that for materials with low-electron mobility the role of the EY mechanism is increased, and the crossover temperature is higher. It has already been demonstrated that for InSb single quantum wells with low-electron mobility the crossover between DP and EY mechanisms occurs around the electron mobility of $1 \text{ m}^2 \text{ V}^{-1} \text{ s}^{-1}$ and could be achieved at 200 K.¹³ For spintronics applications it is essential not only to have long spin lifetime, but also for the spin-FET the DP process should dominate, because an externally applied electric field can change its magnitude through the Rashba effect.¹⁴ This gives us the opportunity to control the electron spin lifetime, especially in NGS, which have a large predicted Rashba effects. The EY process is not strongly affected by the electric field.

III. EXPERIMENT AND RESULTS

Three undoped InAs films of different thicknesses ($d = 0.15, 0.27, \text{ and } 1 \mu\text{m}$) were grown on semi-insulating GaAs(001) substrate by molecular-beam epitaxy (MBE).

A circularly polarized pump-probe experiment was performed to study spin dynamics. The induced-transmission change of the probe beam was measured as a function of the time delay between pump and probe pulses having the same circular polarizations (SCP), and the opposite circular polarizations (OCP). The optical polarization (SCP–OCP)/(SCP+OCP) is proportional to the spin polarization in the sample. The light source was a difference frequency generator, which mixes the signal and the idler beams of an optical parametric amplifier, itself pumped by an amplified Ti:sapphire oscillator. The time resolution of the experiments was about 200 fs. A ZnSe photoelastic modulator was used to modulate the polarization of the pump beam. The detailed description of the experimental technique is given elsewhere.¹⁵ The wavelength was tuned at each temperature to the InAs band edge and was in the range of $3\text{--}3.5 \mu\text{m}$ (although the laser is time-bandwidth limited to $0.3 \mu\text{m}$ width anyway).

The decay of spin population at room temperature as a function of time for undoped InAs films is shown in Fig. 1. The electron-spin lifetime as a function of temperature for all samples is shown in Fig. 2. In addition to thin undoped films, the results for a $3\text{-}\mu\text{m}$ -thick lightly Si-doped ($5.2 \times 10^{16} \text{ cm}^{-3}$) sample (IC313) previously used for doping density dependence investigations¹⁵ are presented as well.

IV. TRANSPORT PROPERTIES

As already mentioned the spin dynamics depend on the charge density and scattering rate. The mobility, μ , and sheet

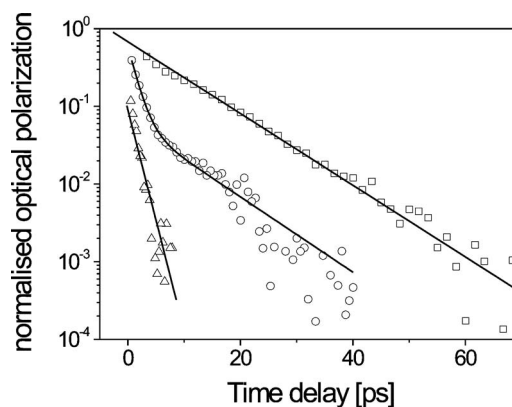


FIG. 1. The time evolution of spin population measured at room temperature for the undoped InAs films of different thicknesses, $0.15 \mu\text{m}$ (triangles), $0.27 \mu\text{m}$ (circles), and $1 \mu\text{m}$ (squares).

carrier concentration, n_s , were obtained by Hall measurements in a cloverleaf van der Pauw geometry. Their temperature dependences in the range $T=4\text{--}300 \text{ K}$ are shown in Fig. 3. The effective three-dimensional (3D) concentration assuming homogeneous material, n_{3D} , is given by n_s/d and is shown for room temperature in Table I.

However, the properties of the InAs films can only be fully understood by taking into account the inhomogeneous depth profiles of the carrier concentration and mobility and the resultant parallel conduction paths. The fall and rise of the carrier density (Fig. 3) is characteristic of material in which both semiconducting and metallic transport processes are occurring. Similar results have been observed for impurity band conduction in Si and Ge (Ref. 16) and more recently in GaN.¹⁷

In addition to the inhomogeneity near the surface due to the accumulation layer, growth on GaAs substrates produces inhomogeneity at the interface. The cross-sectional TEM of the GaAs/InAs interface of one of the available samples is shown in Fig. 4. The dislocation density in the samples appears to be very high for approximately the first $0.1 \mu\text{m}$ of

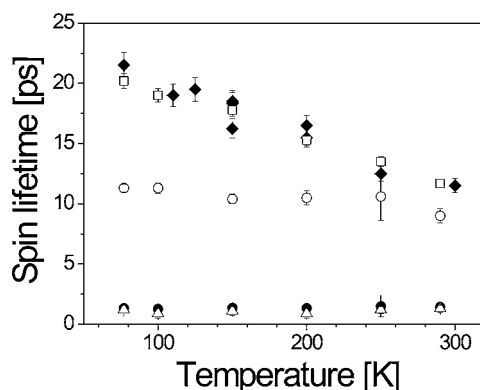


FIG. 2. The temperature dependence of the spin lifetime from the population decay curves $0.15 \mu\text{m}$ (triangles), $0.27 \mu\text{m}$ (circles), and $1 \mu\text{m}$ (squares). In the case of the $0.27 \mu\text{m}$ film the decay has two components; the slow component is shown with open symbols and the fast component with solid symbols. Also shown are data for a doped $3\text{-}\mu\text{m}$ -thick InAs film from Ref. 15 (solid diamonds).

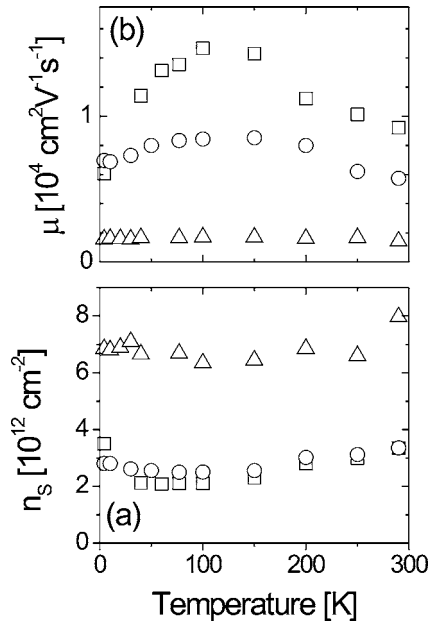


FIG. 3. Temperature dependence of (a) Sheet carrier density n_s and (b) mobility μ for film thicknesses 0.15 μm (triangles), 0.27 μm (squares), and 1.00 μm (circles). Solid symbols are the experimentally measured data. The open circles are the derived data for the semiconducting layer in the 1.00 μm sample after subtraction of the metallic contribution (data are scaled up or down by 10 as indicated). The lines are the fits as described in the text.

growth, but then reduces towards the surface. This produces a corresponding reduction in mobility, most markedly at the interface. We note that the semi-insulating GaAs substrates do not themselves contribute to the transport of the samples, and have been used for InAs growth because they are readily available, are transparent in the spectral region of interest, and offer the possibility of integrating with advanced GaAs technology.

Although the mobility and density profiles are expected to be smoothly varying, we have considered the InAs films on GaAs to consist effectively of three distinct regions: (i) a surface accumulation layer [or two-dimensional electron gas (2DEG)] with high carrier concentration and of order 0.05 μm thick;^{18,19} (ii) an n -type interface layer (at the junction with the substrate) of about 0.1 μm thick, which has a high dislocation density, is also highly degenerate, and has low mobility; and in between them (iii) a central region with comparably low carrier concentration and high mobility. We identify the semiconducting component observed in the transport with the central portion of the film, and the interfaces and surface constitute the metallic regions.

Our analysis of the mobilities and carrier concentrations uses the standard multilayer Hall effect technique, derived from the basic two-layer method of Petritz.²⁰ In this model, the combined effective sheet carrier density, n_s , and average effective mobility, μ , are related to the sheet densities and mobilities in the i component layers, n_s^i and μ_i , by

$$n_s \mu = \sum_i n_s^i \mu_i \quad (3)$$

and

TABLE I. Measured and derived properties of the samples studied. All lengths in units of μm , mobilities in $10^3 \text{ cm}^2 \text{ V}^{-1} \text{ s}^{-1}$, sheet concentrations in 10^{12} cm^{-2} , and 3D concentrations in 10^{16} cm^{-3} .

	Samples		
	U24041	U24T4	U24T24
Measured properties			
Total InAs thickness d	0.15	0.27	1.00
n_s (300 K)	8.1	2.4	3.1
μ (300 K)	1.43	5.75	9.22
n_s (4 K)	6.8	2.9	3.5
μ (4 K)	1.56	6.97	6.08
Derived properties			
Effective average n_{3D} (300 K)	54	9	3.1
Semiconducting n_s (300 K)		0.2 ± 0.2	0.58 ± 0.05
Semiconducting μ (300 K)		10 ± 5	17 ± 2
Semiconducting layer thickness		0.10	0.85
Semiconducting 3D density (300 K)		2.0 ± 2.0	0.7 ± 0.1
Interface n_s	2.5 ± 0.5	2.5 ± 0.5	2.5 ± 0.5
Interface μ	1.5 ± 0.5	1.5 ± 0.5	1.5 ± 0.5
Surface n_s	4.5 ± 0.5	4.5 ± 0.5	4.5 ± 0.5
Surface μ	1.5 ± 0.5	5.0 ± 0.5	5.0 ± 0.5

$$n_s \mu^2 = \sum_i n_s^i \mu_i^2. \quad (4)$$

The left-hand sides of Eqs. (3) and (4) are plotted in Fig. 5. To extract the properties of the semiconducting layer of each film, we make two assumptions. First we assume that the metallic layer properties are independent of temperature, so that they contribute a constant baseline to Fig. 5. This is justified by the fact that the data for the 0.15 μm sample, which is thin enough to have no semiconducting layer are nearly flat. Second, we assume that the semiconducting layers are frozen out at low temperatures, so that the values of the metallic contributions to Fig. 5 are simply determined by the intercepts. After subtraction of the metallic contribution, the remainder is due to the temperature-sensitive semiconducting region, shown in Fig. 6. The strong temperature dependence of Fig. 5 in the case of the 1 μm film implies significant transport through the semiconducting layer, in spite of the very small concentration in comparison with the



FIG. 4. Cross-sectional TEM of GaAs/InAs interface.

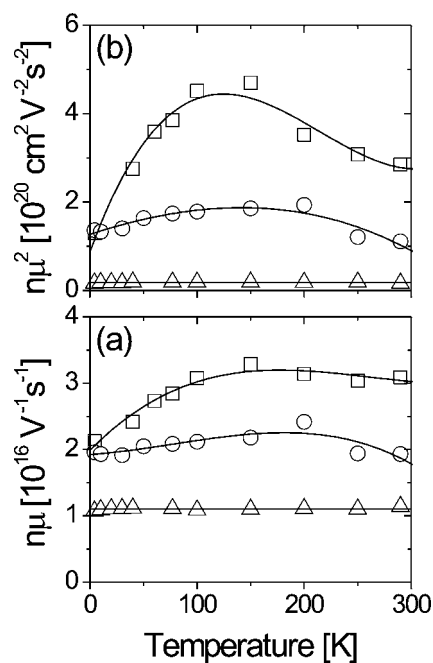


FIG. 5. Temperature dependence of the quantities (a) $n\mu$ and (b) $n\mu^2$, for which contributions from different layers in each sample are additive according to Eqs. (3) and (4). Symbols are the experimentally measured data for film thicknesses 0.15 μm (triangles), 0.27 μm (circles), and 1 μm (squares). The lines are smoothed versions of the data used to extrapolate to the intercept.

metallic layers, which is compensated by the much higher mobility. The product $n\mu$ is proportional to conductivity, and one can see from Fig. 5(a) that the temperature sensitive semiconducting layer carries a maximum of approximately 30% of the current (for temperatures above ≈ 100 K). By contrast the much weaker temperature sensitivity for the 0.27 μm film has made the semiconducting properties much harder to resolve on top of the temperature-independent metallic contribution.

For the thickest sample, the semiconducting concentration follows an Arrhenius behavior, with an activation energy of 8 meV, and a room temperature sheet density of $7 \times 10^{11} \text{ cm}^{-2}$. Above about 50 K the mobility decreases with temperature as expected for lattice scattering, though at low temperatures a switch to impurity scattering is apparent. The room temperature mobility in the thickest film is $\sim 60\%$ of that for bulk material at the same doping level, consistent with the presence of dislocation scattering near to the interface. The room temperature values of the inferred mobility and concentration are given in Table I.

At this point we note that to determine the properties of the semiconducting layer in the 1 μm film, instead of subtracting the assumed metallic contribution as described above, we could have subtracted the experimental values for the 0.27 μm sample to give the properties of a thickness of 0.87 μm of semiconducting material. Since the values of $n\mu$ and $n\mu^2$ for the assumed metallic layer for the 1 μm film and those determined experimentally for the 0.27 μm film (Fig. 5) are nearly equivalent, subtracting either gives almost identical results (though the latter gives more scatter). This gives added confidence in our assumptions. The differential analy-

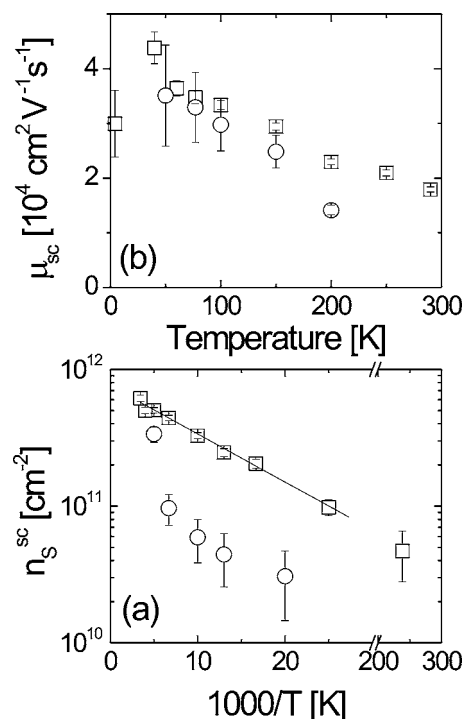


FIG. 6. After subtracting the intercepts from Fig. 5, the remaining temperature-dependent contribution can be rearranged to find the sheet density and mobility of the semiconducting layer, shown in (a) and (b), respectively. Note in (a) the *reciprocal* temperature on the ordinate axis, and the axis break with different scales either side. Symbols are for film thicknesses 0.27 μm (circles), and 1 μm (squares). For the thick sample the density follows a thermal activation behavior (shown by the straight line) with characteristic temperature of ~ 100 K. The error bars include a systematic contribution from the uncertainty in the intercepts of Fig. 5 and are, therefore, small only when the semiconducting contribution is large, compared with the metallic contribution. The points at the ends of the temperature scale for the 0.27 μm sample have been removed because of the large uncertainty.

sis between layers of different thicknesses, has been used previously for InSb layers.^{21,22}

We now attempt to separate the metallic contribution into the surface and interface layer components, though this requires further assumptions that produce high systematic uncertainty. There is a distinct difference in the 4 K metallic properties between the thinnest film and the two thicker ones; the latter have approximately half the sheet density and four times the mobility of the former. We attribute this to the defects from the interface layer having propagated far enough to affect the surface mobility in the thinnest sample. Thus the 0.15 μm film can be treated as approximately uniformly defective, so that the mobilities at the interface and surface are similar and equal to the average ($1.6 \times 10^3 \text{ cm}^2 \text{ V}^{-1} \text{ s}^{-1}$). If we further assume that all metallic layer properties are independent of film thickness (apart from the reduced surface mobility of the thinnest sample), the best fit to the combined metallic contributions deduced above is given in Table I. The surface 2DEG density is very close to

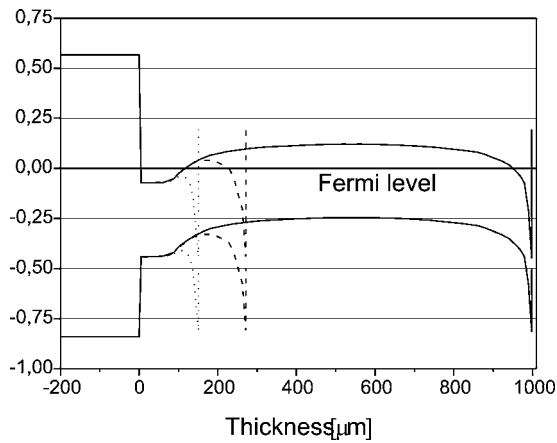


FIG. 7. Theoretical band-bending profiles for the three samples studied here at 300 K.

previously reported values.¹⁹ As already mentioned there is a strong covariance between these parameters and a correspondingly high systematic uncertainty which we have endeavored to indicate in Table I.

These deductions allow an approximate band-bending diagram to be calculated at 300 K using Poisson's equation, and this is shown in Fig. 7 for the three-layer thicknesses studied. Since the exact charge distribution at the interface is unknown, we have represented this by a uniformly doped slab $0.1 \mu\text{m}$ thick, based on the average defected layer thickness, Fig. 4. It can be seen that the overall thickness of the interface layer controls the band edge position in the nominally undoped central region, so that this region should appear more lightly doped in thicker samples. For the thickest film the semiconducting layer sheet density can be converted into an approximate volume figure of $7 \times 10^{15} \text{ cm}^{-3}$ by using a thickness of $0.85 \mu\text{m}$ for the central region, estimated from Fig. 7. For the intermediate thickness sample, using a central layer thickness of $0.10 \mu\text{m}$, we obtain an increased volume density of $2 \times 10^{16} \text{ cm}^{-3}$ because of the increased influence of the accumulation layers.

V. DISCUSSION

The time evolution of the spin population of electrons in the thick, doped sample (IC313) can be described by a single exponential decay with no evidence of the multiple components in the decay that might be expected if several layers of different properties are important. It was found that the DP process is the dominant spin-relaxation mechanism in the temperature range from 77 to 290 K, and that the EY process predicts a much longer lifetime than that observed.¹⁵ The temperature dependence is less strong than that predicted by substituting $E_k = k_B T$ into Eq. (2) because the Fermi energy is very close to the band edge, so that the electron distribution is not fully Boltzmann-like.

The $1 \mu\text{m}$ film also exhibits a single exponential spin decay and similar temperature dependence. This suggests that the spin lifetime in $1 \mu\text{m}$ sample is also due to spin orientation in the bulklike region. The $0.27 \mu\text{m}$ film is found to have two exponential decays in the spin population (Fig.

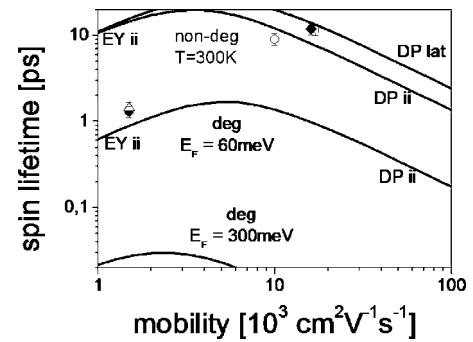


FIG. 8. Spin lifetime as a function of the electron mobility for different electron densities. The experimental data are the room temperature values from Fig. 2 using the same symbols. The lines represent theoretical predictions using Eqs. (1) and (2). At the left (low mobility) EY dominates Eq. (1), and on the right DP dominates Eq. (2). For the nondegenerate model at 300 K ($E_k = kT = 25 \text{ meV}$), appropriate for the central semiconducting region, two versions of the DP prediction are shown for lattice scattering and for ionized impurity scattering. For the degenerate models appropriate for the interface ($E_k = E_F = 60 \text{ meV}$) and surface ($E_k = E_F = 300 \text{ meV}$) we assumed ionized impurity scattering dominates. The predicted surface spin lifetime ($\mu = 5 \times 10^3 \text{ cm}^2 \text{ V}^{-1} \text{ s}^{-1}$) is 0.02 ps (extrapolating the $E_F = 300 \text{ meV}$ curve).

1), and because of its similar magnitude to the thicker sample results we assume that the longer lifetime component is due to the central semiconducting layer.

The thin film results and the short component of the spin lifetime of $0.27 \mu\text{m}$ film are very similar (see Figs. 1 and 2) which suggests that they have the same origin. There is no semiconducting central region in the $0.15 \mu\text{m}$ film so the dynamics must relate to the higher concentration regions. The Fermi energy of the surface inversion layer (of all films) is about 300 meV (see Fig. 7), corresponding to a large Moss-Burstein-shift in the absorption edge. Consequently optical creation of a spin population there is not possible. In addition, while the surface-layer densities are assumed similar, the mobilities differ by more than a factor of 3 between samples, so if this layer were responsible for the observed dynamics, a large difference in magnitude would be seen. On the other hand, the parameters of the electrons in the interface layers are assumed to be the same ($E_F \sim 60 \text{ meV}$), and we, therefore, identify the short spin relaxation component with this layer. The Fermi energy is high in this layer, which reduces the absorption due to the Moss-Burstein shift, but does not forbid optical injection completely, especially in the presence of a strong laser pulse. The relative contribution of the interface layer into a pump-probe signal becomes smaller for thicker samples. That is why we could only see one component in the $1 \mu\text{m}$ film.

Before interpreting the temperature dependences of the short spin lifetimes, let us return to more detail consideration of spin-relaxation mechanisms. As has already been mentioned, the EY mechanism is linearly proportional to the mobility, whereas the DP mechanism is inversely proportional to μ . The crossover between two mechanisms occurs at

$$\mu^{(co)} = \frac{\alpha e \hbar}{\beta m} \sqrt{\frac{A}{QE_G E_k}}. \quad (5)$$

At room temperature, in the nondegenerate semiconducting layer lattice scattering is dominant and $\mu_{lc}^{(co)} = 3 \times 10^3 \text{ cm}^2 \text{ V}^{-1} \text{ s}^{-1}$ at 300 K. The electron mobility is larger than $\mu_{lc}^{(co)}$, which means that the electrons obey the nondegenerate DP spin-relaxation mechanism. In the degenerate interface region impurity scattering is dominant, and the mobility is smaller than $\mu_{ii}^{(co)} = 5 \times 10^3 \text{ cm}^2 \text{ V}^{-1} \text{ s}^{-1}$ at $E_F = 60 \text{ meV}$ (taken from Fig. 7); thus the electron spin lifetime is determined by the EY process. We have summarized these conclusions in Fig. 8.

Extrapolating the degenerate EY process to $E_F = 300 \text{ meV}$, the spin lifetime in the surface layers can be estimated. It is found that at room temperature the spin lifetime of the electrons in the surface layer is around 0.02 ps. The sensitivity of our experiment is not enough to detect this short time. Such a short spin lifetime for the surface layer would not have such serious implication for spintronic devices were it not for the fact that conductivity values produced from the transport analysis (Figs. 5 and 6) show that the majority of the current flows through this layer. Conductivity values

($\propto n_i \mu_i$) calculated from Table I show that even for the thickest film studied (1 μm), the semiconducting region, only carries 30% of the total current, with 10% flowing through the interface layer and a majority 60%, through the surface accumulation layer. Taken together, these facts appear to rule out the usefulness of InAs for spintronic application.

VI. CONCLUSION

To summarize, we have measured the dependence of spin relaxation time at the temperature range from 77 to 300 K for undoped InAs films of different thicknesses from 0.15 to 1 μm . The spin relaxation has several components, and mirrors the transport. The transport properties of InAs films were analyzed by means of the parallel conductivity model. The spin lifetime is very different in the different layers, due to the difference in the mobility and concentration. It was shown that while D'Yakonov-Perel spin dephasing dominates in the low concentration, high mobility semiconducting region in the center of the films, in the low mobility high concentration accumulation layers, Elliott-Yafet spin-flip relaxation dominate, even at room temperature. The spin lifetime in the surface layers was estimated to be much shorter than 1 ps.

¹M. Ziese and M. J. Thornton, *Spin Electronics* (Springer-Verlag, New York, 2001).

²D. D. Awschalom, D. Loss, and N. Samarth, *Semiconductor Spintronics and Quantum Computation* (Springer-Verlag, Berlin, 2002).

³R. Tsai, M. Barsky, J. B. Boos, B. R. Bennett, J. Lee, N. A. Papanicolaou, R. Magno, C. Namba, P. H. Liu, D. Park, R. Grundbacher, and A. Gutierrez, *Technical Digest of the 2003 IEEE GaAs IC Symposium* (2003) (unpublished); T. Ashley, A. B. Dean, C. T. Elliott, G. J. Pryce, A. D. Johnson, and H. Wills, *Appl. Phys. Lett.* **66**, 481 (1995).

⁴M. Zwierzycki, K. Xia, P. J. Kelly, G. E. W. Bauer, and I. Turek, *Phys. Rev. B* **67**, 092401 (2003).

⁵H. H. Wieder, *Appl. Phys. Lett.* **25**, 206 (1974).

⁶H. A. Washburn, J. R. Sites, and H. H. Wieder, *J. Appl. Phys.* **50**, 4872 (1979).

⁷D. C. Tsui, *Solid State Commun.* **9**, 1789 (1971).

⁸O. P. Agnihotri, C. A. Musca, and L. Faraone, *Semicond. Sci. Technol.* **13**, 839 (1998).

⁹M. I. D'yakonov and V. I. Perel', *Sov. Phys. Solid State* **13**, 3023 (1972).

¹⁰R. J. Elliot, *Phys. Rev.* **96**, 266 (1954).

¹¹G. L. Bir, A. G. Aronov, and G. E. Pikus, *Sov. Phys. JETP* **42**, 705 (1976).

¹²P. H. Song and K. W. Kim, *Phys. Rev. B* **66**, 035207 (2002).

¹³K. L. Litvinenko, B. N. Murdin, J. Allam, C. R. Pigeon, M. Bird, K. Morris, W. Branford, S. K. Clowes, L. F. Cohen, T. Ashley, and L. Buckle, *New J. Phys.* **8**, 49 (2006).

¹⁴W. Zawadzki and P. Pfeffer, *Semicond. Sci. Technol.* **19**, R1-R17 (2004).

¹⁵B. N. Murdin, K. Litvinenko, J. Allam, C. R. Pidgeon, M. Bird, K. Morrison, T. Zhang, S. K. Clowes, W. R. Branford, and L. F. Cohen, *Phys. Rev. B* **72**, 085346 (2005).

¹⁶E. Conwell, *Phys. Rev.* **103**, 51 (1956).

¹⁷R. J. Molnar, T. Lei, and T. D. Moustakis, *Appl. Phys. Lett.* **62**, 72 (1993).

¹⁸P. D. Wang, S. N. Holmes, Tan Le, R. A. Stradling, I. T. Ferguson, and A. G. de Oliveira, *Semicond. Sci. Technol.* **7**, 767 (1992).

¹⁹H. A. Washburn, J. R. Sites, and H. H. Wieder, *J. Appl. Phys.* **50**, 4872 (1979).

²⁰R. L. Petritz, *Phys. Rev.* **110**, 1254 (1958).

²¹T. Zhang, S. K. Clowes, M. Debnath, A. Bennett, C. Roberts, J. J. Harris, R. A. Stradling, L. F. Cohen, T. Lyford, and P. F. Fewster, *Appl. Phys. Lett.* **84**, 4463 (2004).

²²J. J. Harris, T. Zhang, W. R. Branford, S. K. Clowes, M. Debnath, A. Bennett, C. Roberts, and L. F. Cohen, *Semicond. Sci. Technol.* **19**, 1406 (2004).